



Article

# The Integrated Stress Response Is Tumorigenic and Constitutes a Therapeutic Liability in Somatotroph Adenomas

Zhenye Li <sup>1,†</sup>, Yiyuan Chen <sup>1,2,†</sup>, Xiaohui Yao <sup>2,3</sup>, Qian Liu <sup>2</sup>, Haibo Zhu <sup>1</sup>, Yazhuo Zhang <sup>1,2</sup>, Jie Feng <sup>2,\*</sup> and Hua Gao <sup>2,4,5,\*</sup>

<sup>1</sup> Beijing Tiantan Hospital, Capital Medical University, Beijing 100070, China

<sup>2</sup> Beijing Neurosurgical Institute, Capital Medical University, Beijing 100070, China

<sup>3</sup> Shanxi Provincial People's Hospital, Taiyuan 030000, China

<sup>4</sup> China National Clinical Research Center for Neurological Diseases, Beijing 100070, China

<sup>5</sup> Key Laboratory of Central Nervous System Injury Research, Beijing 100070, China

\* Correspondence: fj79330@163.com (J.F.); huagao\_bj@163.com (H.G.)

† These authors contributed equally to this work.

**Abstract:** Somatotroph adenomas are the leading cause of acromegaly, with the nearly sparsely granulated somatotroph subtype belonging to high-risk adenomas, and they are less responsive to medical treatment. The integrated stress response (ISR) is an essential stress-support pathway increasingly recognized as a determinant of tumorigenesis. In this study, we identified the characteristic profiling of the integrated stress response in translocation and translation initiation factor activity in somatotroph adenomas, normal pituitary, or other adenoma subtypes through proteomics. Immunohistochemistry exhibited the differential significance and the priority of eukaryotic translation initiation factor 2 $\beta$  (EIF2 $\beta$ ) in somatotroph adenomas compared with gonadotroph and corticotroph adenomas. Differentially expressed genes based on the level of EIF2 $\beta$  in somatotroph adenomas were revealed. MetaScape pathways showed that EIF2 $\beta$  was involved in regulating growth and cell activation, immune system, and extracellular matrix organization processes. The correlation analysis showed Spearman correlation coefficients of  $r = 0.611$  ( $p < 0.001$ ) for EIF2 $\beta$  and eukaryotic translation initiation factor 2 alpha kinase 1 (HRI),  $r = 0.765$  ( $p < 0.001$ ) for eukaryotic translation initiation factor 2 alpha kinase 2 (PKR),  $r = 0.813$  ( $p < 0.001$ ) for eukaryotic translation initiation factor 2 alpha kinase 3 (PERK),  $r = 0.728$  ( $p < 0.001$ ) for GCN2, and  $r = 0.732$  ( $p < 0.001$ ) for signal transducer and activator of transcription 3 (STAT3). Furthermore, the invasive potential in patients with a high EIF2 $\beta$  was greater than that in patients with a low EIF2 $\beta$  (7/10 vs. 4/18,  $p = 0.038$ ), with a lower immune-cell infiltration probability ( $p < 0.05$ ). The ESTIMATE algorithm showed that the levels of activation of the EIF2 pathway were negatively correlated with the immune score in somatotroph adenomas ( $p < 0.001$ ). In *in vitro* experiments, the knockdown of EIF2 $\beta$  changed the phenotype of somatotroph adenomas, including cell proliferation, migration, and the secretion ability of growth hormone/insulin-like growth factor-1. In this study, we demonstrate that the ISR is pivotal in somatotroph adenomas and provide a rationale for implementing ISR-based regimens in future treatment strategies.

**Keywords:** somatotroph adenomas; integrated stress response; tumorigenesis; EIF2



**Citation:** Li, Z.; Chen, Y.; Yao, X.; Liu, Q.; Zhu, H.; Zhang, Y.; Feng, J.; Gao, H. The Integrated Stress Response Is Tumorigenic and Constitutes a Therapeutic Liability in Somatotroph Adenomas. *Int. J. Mol. Sci.* **2022**, *23*, 13067. <https://doi.org/10.3390/ijms232113067>

Academic Editors: Salvatore Maria Corsello and Rosa Maria Paragliola

Received: 31 August 2022

Accepted: 25 October 2022

Published: 28 October 2022

**Publisher's Note:** MDPI stays neutral with regard to jurisdictional claims in published maps and institutional affiliations.



**Copyright:** © 2022 by the authors. Licensee MDPI, Basel, Switzerland. This article is an open access article distributed under the terms and conditions of the Creative Commons Attribution (CC BY) license (<https://creativecommons.org/licenses/by/4.0/>).

## 1. Introduction

Somatotroph adenomas are a kind of functional pituitary adenomas that cause acromegaly due to the excessive secretion of growth hormone (GH) and insulin-like growth factor (IGF-1) [1]. Excess GH/IGF-1 in somatotroph adenoma patients causes the overgrowth of some tissues and multiple metabolic abnormalities by affecting body composition, protein dynamics, and molecular mechanisms in adults [2]. The mortality risk is related to the duration of the illness before diagnosis and the lesional degree of cardiovascular disease and diabetes at the time of diagnosis [3]. Improvements in diagnostic modalities have increased the prevalence of somatotroph adenomas through the identification of active

acromegaly (high IGF-1 and/or GH levels) in clinically asymptomatic patients, also called silent somatotroph adenomas [3]. Compared to other subtypes, up to 50% of somatotroph adenoma patients have clear phenotypic changes, whereas another ~50% have either mild symptoms or are visibly asymptomatic for metabolic abnormality, including polyamine anabolism and sugar anabolism [4]. Initial therapy generally constitutes transsphenoidal surgery, although the remission rate is approximately 50%; somatostatin analog (SSA) therapy is reserved for cases not cured by surgery [5]. The WHO 2017 classification suggests that subtypes of pituitary adenoma, such as male lactotrophs, silent corticotroph and Crouse cells, sparsely granulated somatotrophs, and silent plurihormonal POU Class 1 Homeobox 1-positive tumors, should be considered as “high risk” tumors [6].

The integrated stress response (ISR) is an essential stress-support pathway increasingly recognized as a determinant of tumorigenesis via tuning protein synthesis rates [7]. The various stresses are sensed by four specialized kinases—eukaryotic translation initiation factor 2 alpha kinase 1 (HRI), eukaryotic translation initiation factor 2 alpha kinase 2 (PKR), eukaryotic translation initiation factor 2 alpha kinase 3 (PERK), and eukaryotic translation initiation factor 2 alpha kinase 4 (GCN2)—that converge on the phosphorylation of a single serine on the eukaryotic translation initiation factor eIF2 [8]. The salient feature of ISR signaling lies in the modulation of the cellular concentration of the ternary complex (TC), which is composed of the heterotrimeric eukaryotic translation initiation factor and eukaryotic translation initiation factor 2 (EIF2), consisting of an  $\alpha$ ,  $\beta$ , and  $\gamma$  subunit in equal molar amounts [9]. Phosphorylation of the eIF2 subunit regulates the heterotrimer activity [10]. Oncogenic roles of eIF2 $\alpha$  are well-known in chronic myeloid leukemia [11], colorectal cancer [12], prostate cancer [13], and so on. eIF2 $\beta$  forms part of the nucleotide-binding pocket in eukaryotes and appears to bind GTP or GDP [14]. Integrated genomic data in breast cancer has shown that eIF2 $\beta$  is highly amplified and correlates to the aggressive behavior of luminal breast tumors [15]. eIF2 $\gamma$  has a catalytic site for GTPase activity and is involved in binding of the ternary complex to mRNA; the eIF2 $\gamma$  variant is associated with hypothalamo-pituitary development, hypopituitarism, and pancreatic dysfunction and glucose regulation [16]. The ISR is a double-edged sword with both pro-survival and pro-death activities, and regulation of ISR signaling components is a promising strategy in cancer therapy [17,18].

While the ISR is upregulated in many cancers, its precise function in tissue-specific cancer initiation and progression remains poorly understood [19]. In this study, we explored somatotroph adenomas using multi-omic methods and showed the unique characteristics of the eIF2 pathway and ribosome-related genes in somatotroph adenoma patients compared to patients with other subtypes of pituitary adenomas. We demonstrated the relationship of the ISR with disease phenotype and immune cell infiltration in somatotroph adenomas together with the strong therapeutic benefits of its pharmacological inhibition.

## 2. Results

### 2.1. Clinical Characteristics of Patients

Our study included 144 patients: 33 somatotroph adenomas, 75 gonadotroph adenomas, and 36 corticotroph adenomas (Table 1). There were 79 males and 65 females, with an average age of  $49.1 \pm 1.01$  years (range: 17–69). The average tumor size was  $11.24 \pm 1.53$  cm<sup>3</sup> (range: 0.74–42.76), including 2 microadenomas, 124 macroadenomas, and 18 giant adenomas. According to Knosp staging, there were 67 invasive cases and 77 non-invasive cases. The average follow-up time was  $56.6 \pm 10.7$  months (range: 42–78), with five-year recurrence rates as follows: 7/33 (21.2%) for somatotroph adenomas, 10/75 (13.3%) for gonadotroph adenomas, and 13/36 (36.1%) for corticotroph adenomas. There were more female patients and a greater invasion and recurrence chance in corticotroph adenoma and more younger patients with somatotroph adenoma ( $p < 0.05$ ).

**Table 1.** Clinicopathological features of patients with pituitary adenomas.

Variable	CORT	GONA	SOMA	<i>p</i> Value
Sex				<0.001
Male	8	55	16	
Female	28	20	17	
Age	50.75 ± 2.10	52.85 ± 1.28	43.58 ± 1.89	<0.001
Tumor size				0.523
Micro	0	7	1	
Macro	29	66	29	
Giant	7	8	3	
Tumor volume (cm <sup>3</sup> )	14.39 ± 2.69	11.94 ± 2.62	6.89 ± 1.44	0.234
Invasion				0.004
No	11	46	20	
Yes	26	29	13	
Recurrence				0.022
No	23	65	26	
Yes	13	10	7	

Note: CORT: corticotroph adenoma; GONA: gonadotroph adenoma; SOMA: somatotroph adenoma.

In this cohort, the gender balance was 8:28 in CORT, 55:20 in GONA, and 16:17 in SOMA ( $p < 0.001$ ). That is, there were more female patients in CORT and more male patients in GONA. The average age was  $50.75 \pm 2.10$  in CORT,  $52.85 \pm 1.28$  in GONA, and  $43.58 \pm 1.89$  in SOMA ( $p < 0.001$ ). The youngest patients were in the SOMA group, and there was no statistical difference in age between CORT and GONA. The recurrence rate was 13/36 (36.1%) in CORT, 10/75 (13.3%) in GONA, and 47/33 (21.2%) in SOMA ( $p < 0.001$ ). The worst prognosis was in CORT compared with GONA and SOMA.

## 2.2. Characteristic Profiling in Somatotroph Adenomas Compared to Normal Pituitary, Corticotroph Adenomas, and Gonadotroph Adenomas

Differentially expressed proteins were identified by nanoLC-MS/MS among five normal pituitary tissues, five somatotroph adenomas, five gonadotroph adenomas, and five corticotroph samples. Proteomics analysis identified 46,383 peptides that mapped to 4751 proteins. A total of 274 proteins were differentially expressed ( $p < 0.05$ , with an iTRAQ ratio  $>1.5$  or  $<0.7$ ); 130 were upregulated; and 144 were downregulated in somatotroph adenomas, as shown in Figure 1A,B. Using the Metascape database, pathway and process enrichment analyses showed that the top three pathways were SRP-dependent cotranslational protein targeting to the membrane, peptide chain elongation, and eukaryotic translation elongation, as shown in Figure 1C. The top three GO biological processes were cytoplasmic translation, protein localization to the plasma membrane, and regulation of neurotransmitter levels, as shown in Figure 1D. The summary of enrichment analyses in TRRUST showed that the differentially expressed proteins were regulated by STAT3, REST, TFAP2A, SNAI1, etc., as depicted in Figure 1E.

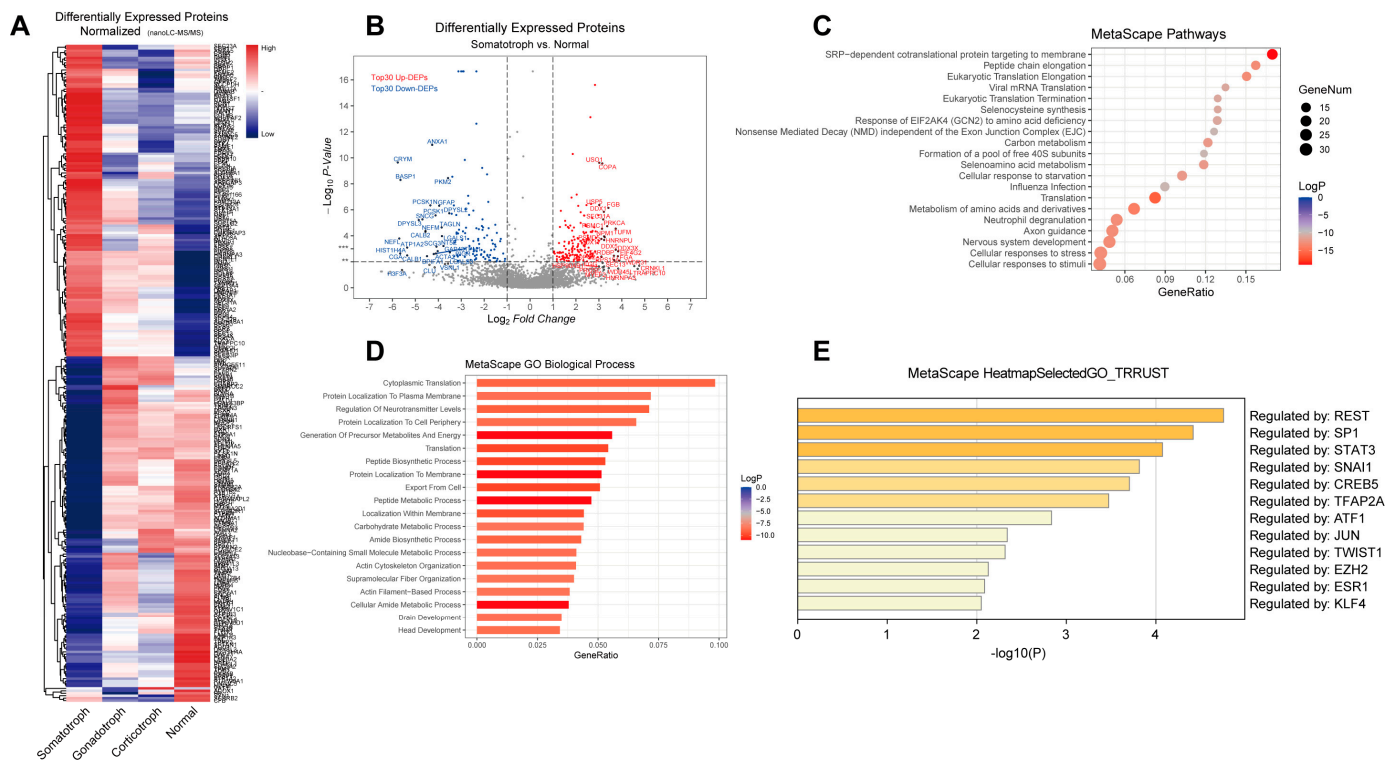


**Figure 1.** Proteomics analysis of normal pituitary gland and corticotroph adenomas, gonadotroph adenomas, and somatotroph adenomas. (A): A heatmap of differentially expressed proteins (FC > 1.5 or FC < 0.67 and FDR q < 0.1). High expression is shown in red; low expression is shown in blue. (B): Volcano map of differentially expressed proteins. \*\*  $p < 0.01$ , \*\*\*  $p < 0.001$  (C): KEGG pathway analysis based on differentially expressed proteins. (D): The most enriched GO terms. (E): Enrichment analysis in TRRUST showing differentially expressed proteins regulated by STAT3, REST, TFAP2A, and SNAI1 based on the Metascape database.

Somatotroph adenoma and lactotroph both belong to the PIT-1 lineages of PAs. In this study, we analyzed the difference between somatotroph and macro-lactotroph adenomas, as shown in Figure S1. The volcano map shows the top 20 DEGs in Figure S1A. Using the Metascape database, DEG pathway enrichment shows the top 10 GO biological processes in Figure S1B and the top 10 KEGG pathways in Figure S1C,D.

EIF2 is a key component of the ternary complex whose role is to deliver initiator tRNA into the ribosome. Mass-spectrometric data showed increased subunit  $\alpha/\beta$  and reduction in  $\gamma$  subunit, mainly subunit  $\beta$ . Immunohistochemistry exhibited the differential significance and the priority of EIF2 $\beta$  in somatotroph adenomas compared with gonadotroph and corticotroph adenomas, as depicted in Figure 2.

Correlation analysis showed that the correlation coefficient of EIF2 $\beta$  and STAT3 was 0.541 (Figure S2) ( $p < 0.001$ ).

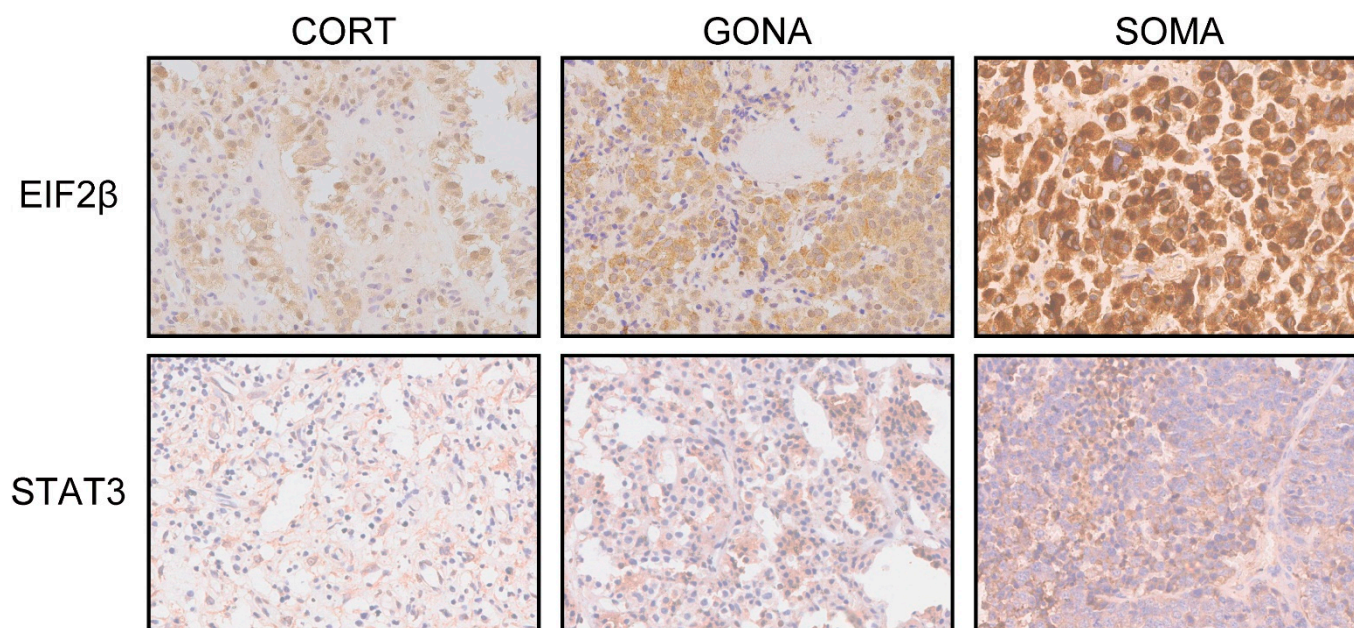


**Figure 2.** Immunohistochemistry images of EIF2 $\beta$  and STAT3 in corticotroph adenomas, gonadotroph adenomas, and somatotroph adenomas. CORT: corticotroph adenomas; GONA: gonadotroph adenomas; SOMA: somatotroph adenomas ( $\times$ : 40 fold).

### 2.3. Differentially Expressed Gene-Enrichment Analysis between EIF2 $\beta$ Groups

According to the H-score of EIF2 $\beta$  (H-score: 114), patients with somatotroph adenomas were divided into a high-EIF2 $\beta$  group ( $n = 10$ ) and a low-EIF2 $\beta$  group ( $n = 18$ ); six samples were excluded because of staining loss. Based on different levels of EIF2 $\beta$ , there were 244 differentially expressed genes (I fold change  $\geq 1$ ,  $p < 0.05$ ). The top three pathways were cytokine signaling in the immune system, hemostasis, and extracellular matrix organization (Figure 3A). The top three GO biological processes were complement activation, classical pathway complement activation, and humoral immune response mediated by circulating immunoglobulins (Figure 3B). Correlation analysis showed the following Spearman correlation coefficients: EIF2 $\beta$  and HRI ( $r = 0.611$ ,  $p < 0.001$ ), PKR ( $r = 0.765$ ,  $p < 0.001$ ), PERK ( $r = 0.813$ ,  $p < 0.001$ ), GCN2 ( $r = 0.728$ ,  $p < 0.001$ ), and STAT3 ( $r = 0.732$ ,  $p < 0.001$ ) (Figure 3C).

Furthermore, we analyzed the clinical relevance of EIF2 $\beta$  in 28 patients with somatotroph adenoma (Table 2). Patients with a high EIF2 $\beta$  had a greater invasive potential ( $p = 0.038$ ). There was a tendency toward a more sparsely granulated adenoma phenotype in 28 somatotroph adenoma patients with a high EIF2 $\beta$  than in patients with a low EIF2 $\beta$ .

**Table 2.** Clinically pathological features of patients with somatotroph adenoma.

Variable	EIF2 $\beta$		p Value
	High	Low	
Sex			1
Male	5	8	
Female	5	8	
Age	42.4 $\pm$ 2.54	43.71 $\pm$ 2.87	0.76
Tumor size			0.274
Micro	0	1	
Macro	10	15	
Giant	0	3	
Tumor volume (cm <sup>3</sup> )	3.49 $\pm$ 0.66	7.76 $\pm$ 2.33	0.193

Table 2. Cont.

Variable	EIF2 $\beta$		p Value
	High	Low	
Invasion			0.038
No	3	14	
Yes	7	4	
Recurrence			1
No	7	14	
Yes	3	4	
Granulate Sparseness			0.09
Density	8	7	
Density	2	11	
HGH (folds/normal)	4.38 $\pm$ 1	2.32 $\pm$ 0.60	0.071

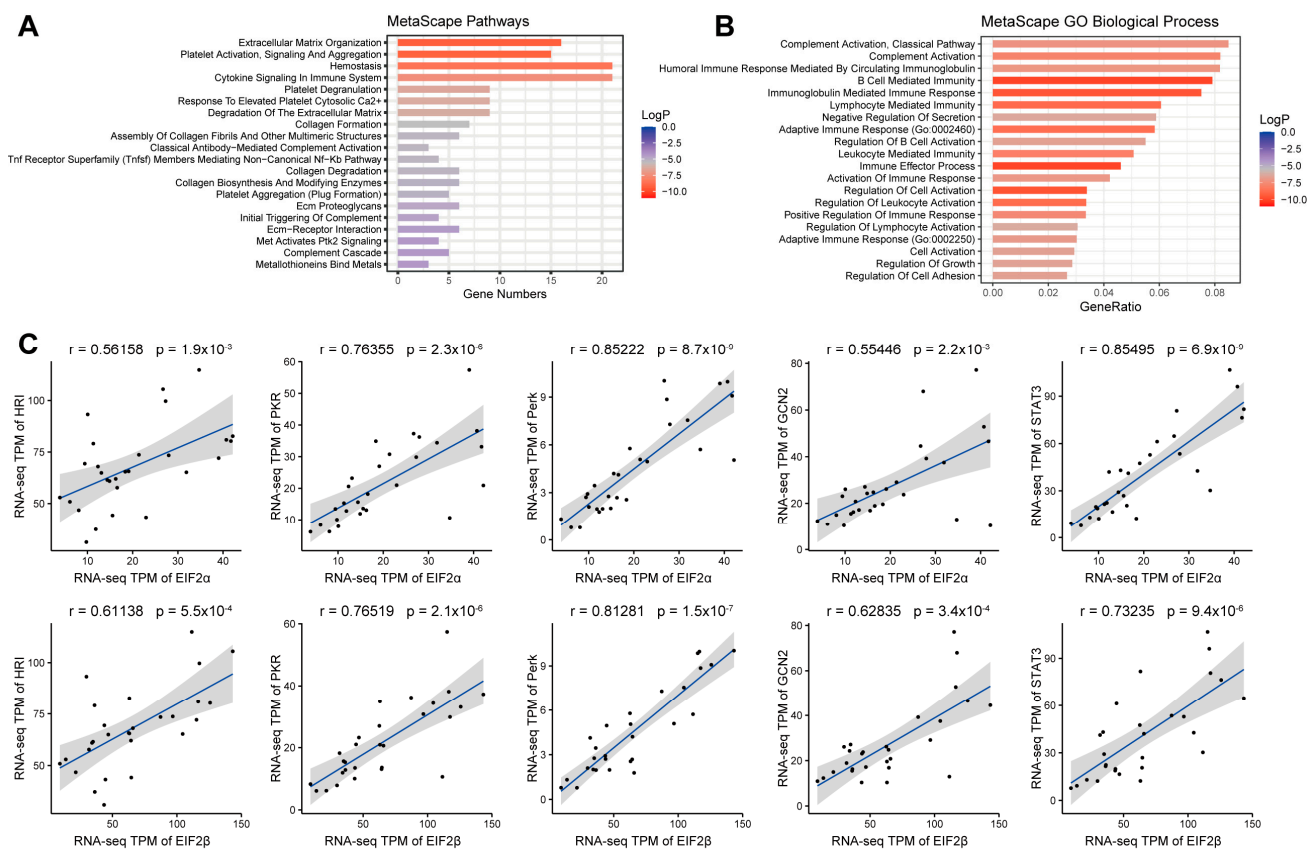


**Figure 3.** Differential gene-enrichment analyses of different EIF2 $\beta$  groups in 28 patients with somatotroph adenomas. (A,B): Metascape enrichment analysis, including pathways and GO terms. (C): Correlation analysis of EIF2 $\alpha/\beta$  and EIF2AK1-4 and STAT3.

#### 2.4. Immunologic Signatures in Patients with Somatotroph Adenomas

First, we described the immune cell types and percentages with a heatmap for patients with somatotroph adenomas (Figure 4A). The associations between the infiltrate levels of immune cell signatures and levels of EIF2 $\beta$  are illustrated in Figure 4B; there was a statistically significant difference in lymphocytes, macrophages, and dendritic cells between patients with a high EIF2 $\beta$  and patients with a low EIF2 $\beta$  ( $p < 0.05$ ) (Figure 4C). Moreover, according to the unpaired t test, there were significant differences in the immune score ( $p = 0.020$ ) and ESTIMATE score ( $p = 0.024$ ) between patients with a high EIF2 $\beta$  and patients with a low EIF2 $\beta$  (Figure 4D).



infiltration probability (24/69 vs. 13/75,  $p = 0.017$ ) in functional pituitary adenomas than in non-functional pituitary adenomas.

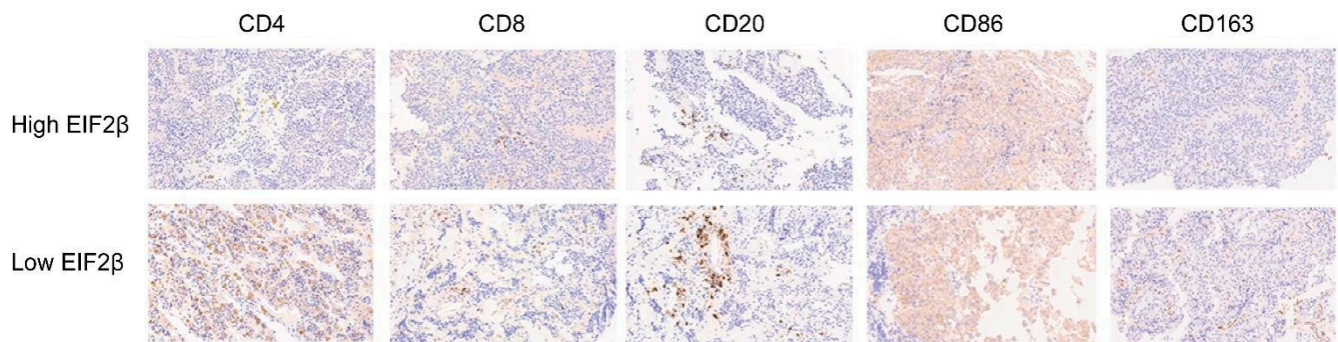


**Figure 5.** Immunohistochemistry images of CD4, CD8, CD20, CD86, and CD163 staining in the high- and low-EIF2 $\beta$  patient groups ( $\times$ : 40 fold).

### 2.6. Effects of RNAi-EIF2 $\beta$ on Cell Proliferation and Growth Hormone Release by GH3 Cells

To test the role of EIF2 $\beta$  in somatotroph adenomas, we constructed the RNA interference fragments of EIF2 $\beta$  and packaged the viral vectors. The interfering efficiency of shRNA1–4 were  $0.97 \pm 0.15$ ,  $0.57 \pm 0.02$ ,  $0.47 \pm 0.03$ , and  $0.91 \pm 0.19$ -fold, respectively, of control GH3 cells after 72 h transient transfection (Figure 6A) ( $p < 0.05$ ). Western blot experiments also showed the same tendency (Figure 6B). The sh2 and sh3 fragments were used in further experiments. The cell viabilities in RNAi groups were  $78.4 \pm 4.7\%$  and  $84.5 \pm 5.1\%$  of that in the control group after 24 h infection,  $67.3 \pm 3.9\%$  and  $71.5 \pm 4.1\%$  after 48 h infection, and  $60.4 \pm 3.8\%$  and  $65.2 \pm 3.7\%$  after 72 h infection, respectively (Figure 6C,  $p < 0.05$ ). ELISA showed that GH levels in the cell culture were  $5.7 \pm 1.1$  ng/mL and  $6.1 \pm 0.9$  ng/mL in the RNAi-EIF2 $\beta$  groups compared with  $11.7 \pm 0.7$  ng/mL in the control GH3 group ( $p < 0.05$ ) after 72 h treatment (Figure 6D). IGF-1 levels in the cell culture were  $7.7 \pm 1.2$  ng/mL and  $9.2 \pm 1.1$  ng/mL in the RNAi-EIF2 $\beta$  groups compared with  $16.3 \pm 0.9$  ng/mL in the control group ( $p < 0.05$ ) after 72 h treatment (Figure 6E). Transwell experiments showed that the trans-membrane-positive cells in the RNAi-sh2 group ( $226 \pm 27$ /high field) and RNAi-sh3 group ( $254 \pm 32$ /high field) were reduced compared with the control group ( $403 \pm 67$ /high field) (Figure 6F). We also found a decline in STAT3 and STAT5b in the sh2 and sh3 groups (Figure 6G).

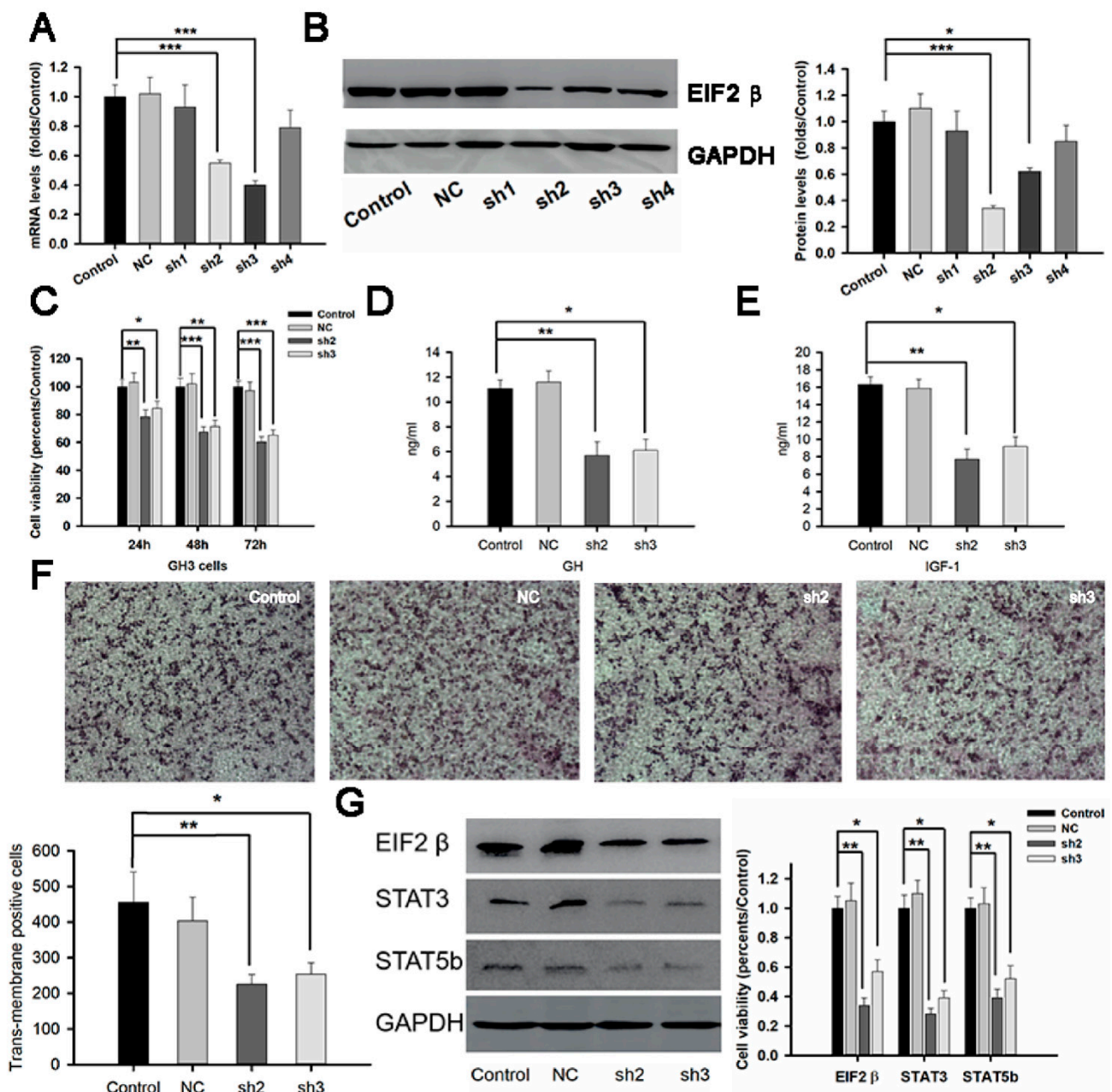


**Figure 6.** RNAi-EIF2β inhibited cell proliferation, growth hormone secretion, and invasion in vitro. (A,B): RT-PCR and Western blot experiments filtered the effective interference fragments of EIF2β in GH3 cells. (C): sh2-EIF2β and sh3-EIF2β reduced the cell viability of GH3 cells in a time-dependent manner. (D): sh2-EIF2β and sh3-EIF2β decreased growth hormone (GH) in GH3 cells. (E): sh2-EIF2β and sh3-EIF2β decreased insulin-like growth factor 1 (IGF-1) in GH3 cells. (F): sh2-EIF2β and sh3-EIF2β decreased trans-membrane-positive cells after 24 h treatment. (G): sh2-EIF2β and sh3-EIF2β reduced protein levels of STAT3 and STAT5b after 24 h treatment. \* Compared to control group  $p < 0.05$  \*\*  $p < 0.01$  \*\*\*  $p < 0.001$ .

### 3. Discussion

Somatotroph adenomas usually induce a decrease in body fat, osteoporosis, and increase water retention. Recent studies suggest that abnormal fat metabolism promotes protein anabolism and relieves amino acid oxidation. Protein synthesis dysregulation is a burgeoning field in cancer biology. The ISR is an essential stress-support pathway, increasingly recognized as a determinant of tumorigenesis by fine-tuning protein-synthesis rates. Translation initiation lies downstream to deregulated signal pathways in cancer

and is regulated by activated oncogenes or mutated tumor suppressors. Therefore, controlling protein synthesis has significant potential for developing innovative therapy in somatotroph adenomas.

In this study, we found significant differences in the eIF2 pathway in somatotroph adenomas compared to normal pituitary and other subtypes of pituitary adenomas through multi-omics analysis. Furthermore, we evaluated the effects of the eIF2 pathway on cell proliferation, invasion, and growth hormone release through *ex vivo* experiments.

Our understanding of the central mechanisms that govern the ISR has advanced vastly. The ISR's central regulatory hub lies in the EIF2-EIF2B complex, which controls the formation of the eEIF2/GTP/methionyl-initiator tRNA TC, a prerequisite for initiating new protein synthesis [7]. EIF2 and EIF2B are complex proteins of three ( $\alpha$ - $\gamma$ ) and five ( $\alpha$ - $\epsilon$ ) nonidentical subunits, respectively [20]. Through integrated multi-omics analysis, we found an abnormally increased profile of ribosomal proteins in somatotroph adenomas compared with normal pituitary glands or other subtypes of pituitary adenomas. In the diversity of differentially expressed proteins, the top three pathways were: SRP-dependent cotranslational protein targeting the membrane, peptide chain elongation, and eukaryotic translation elongation by KEGG pathway enrichment, as shown in Figure 1C. Moreover, we found an imbalance in the EIF2 complex in somatotroph adenomas, i.e., increased  $\alpha/\beta$  subunit and reduction in the  $\gamma$  subunit of eIF2.

Oncogenic roles of eIF2 $\alpha$  have been extensively studied in several human cancers [21]; however, few studies demonstrate the roles of eIF2 $\beta$  in carcinogenesis. An integrated genomic search of novel therapeutic targets for breast cancer indicated that eIF2 $\beta$  is highly amplified in luminal breast tumors, which are an aggressive subtype of breast tumors [22]. In *in vitro* experiments, the knockdown of eIF2 $\beta$  manipulations induced G1 cell cycle arrest in both NCI-H358 and NCI-H460 cells [23]. Deleting the polylysine stretches in the amino-terminal region of eIF2 $\beta$  decreased protein synthesis, inhibited cell proliferation and viability, increased cell death, and induced G2 cell cycle arrest in Hek293TetR cells [24]. Interestingly, we noticed that the levels of EIF2 $\beta$  in somatotroph adenomas were related to the disease phenotype. Patients with a high EIF2 $\beta$  had a higher invasive potential and greater chances of sparsely granulated tumors than patients with low immune-cell infiltration with low EIF2 $\beta$ . The phosphorylation of eIF2 $\alpha$  is carried out by a family of four kinases, PERK, PKR, GCN2, and HRI, which primarily respond to a distinct type of stress or stresses [25]. In this study, we observed a high correlation between EIF2 $\alpha/\beta$  and PKR and PERK expression, suggesting that simultaneous upregulation of these molecules increases translation initiation, contributing to enhanced synthesis and secretion of GH/IGF-1 by somatotroph tumor cells. We found a decrease in cell viability and the level of GH and IGF-1 in the cell culture supernatant of GH3 cells in both sh2-EIF2 $\beta$  and sh3-EIF2 $\beta$  groups.

Enrichment analysis in TRRUST showed that the differentially expressed proteins were regulated by STAT3, REST, TFAP2A, SNAI1, etc. It was reported that STAT3 specifically binds the GH promoter and induces transcription in the GH3 cell line [26]. Additionally, C188-9, an inhibitor of STAT3, could downregulate the levels of eIF2 and STAT3 in GH3 cell lines. We confirmed a positive correlation between EIF2 $\beta$  and STAT3 based on transcriptome data and immunohistochemistry staining. *In vitro* experiments verified that RNAi-EIF2 $\beta$  relieved cell proliferation, invasion, and secretion of GH/IGF-1. Western blot experiments also verified the relationship between EIF2 $\beta$  and STAT3. We hypothesized that EIF2 $\beta$  was mainly involved in tumor-related pathways in somatotroph adenomas, including the cell adhesion molecule pathway and the JAK-STAT signaling pathway. We speculated that eIF2 $\beta$  might inhibit T cell-mediated immunity by promoting the Treg response. In addition, the expression of eIF2 $\beta$  was positively correlated with STAT3 and STAT5b. Related studies have shown that some signaling molecules are involved in the M2 polarization of macrophages, such as PI3K/AKT-ERK signaling, STAT3, HIF1 $\alpha$ , and STAT6. These results suggested that eIF2 $\beta$  might regulate tumor macrophage infiltration, affecting the tumor microenvironment.

The tumor immune microenvironment is increasingly being recognized as a key contributor to tumorigenesis and tumor progression and recurrence. Cancer cells, stromal cells, and immune cells, along with their extracellular factors, have profound effects on either promoting or repressing anti-cancer immunity. These effects were mostly detected by immunohistochemistry; immune cell infiltration varied greatly among samples, which indicated that pituitary-hormone-secreting adenomas have substantial heterogeneity. For example, it has been reported that CD68+ macrophage infiltration was higher than that in corticotroph adenomas and densely granulated somatotroph adenomas [27]. In this study, we found a greater probability of immune cell infiltration in corticotroph adenomas and somatotroph adenomas compared with gonadotroph adenomas. Since corticotroph adenomas and somatotroph adenomas have greater invasive potential, we speculated that immune cell infiltration was related to invasive behavior. However, we found a negative relationship between the levels of eIF2 $\beta$  and immune score in 28 patients with somatotroph adenoma based on the “ESTIMATE” algorithm, which was further validated by immunohistochemistry data. The enriched GO terms by DEG analysis for biological processes were complement activation, classical pathway complement activation, and humoral immune response mediated by circulating immunoglobulins, whereas KEGG pathway terms enriched by DEG analysis were cytokine signaling in the immune system, hemostasis, and extracellular matrix organization; these may all have roles in the modulation of inflammatory infiltration in tumor tissue. The specific mechanism by which inflammatory infiltration leads to tumor invasion requires further investigation; this may also be relevant for further research into and development of targeted drugs for somatotroph adenomas.

However, our study has some limitations. First, the small sample size may have contributed to a bias error; the relationship between eIF2 $\beta$  and sparse granularity needs further confirmation in large samples. Moreover, the transcriptome data analyzed were generated through bulk RNA sequencing; bulk sequencing is likely to cause loss of some information because of the heterogeneous nature of tumor tissues, and this may be explored in more detail with single-cell RNA-seq techniques.

In conclusion, in the present study, we uncovered the unique characteristics of the eIF2 complex and abnormal integrated stress response through omics data in somatotroph adenoma patients. Furthermore, we characterized the landscape of the somatotroph adenoma microenvironment using different methodologies, including immunohistochemistry and transcriptomics. We speculated that eIF2 $\beta$  promoted the synthesis and secretion of GH/IGF-1 in somatotroph tumor cells and inhibited immune cell infiltration.

#### 4. Material and methods

##### 4.1. Patient Sample Acquisition and Cell Lines

All tumor samples were obtained following transsphenoidal surgery performed at Beijing Tiantan Hospital, Beijing, China, from May 2015 to December 2020. Fresh tumor samples were stored in liquid nitrogen. A total of 144 patient samples (age range: 17–69 years) were diagnosed as pituitary adenomas, including 33 somatotroph adenomas, 75 gonadotroph adenomas, and 36 corticotroph adenomas. The pituitary adenoma types were diagnosed according to the 2017 World Health Organization classification of tumors of endocrine organs, including pituitary transcription factors and hormone content, by immunohistochemistry staining. Somatotroph adenomas are divided into two distinct and clinically relevant histologic subtypes, densely and sparsely granulated, based on the density of GH-containing secretory granules and the presence of fibrous bodies. Five normal pituitary glands were obtained from a donation program. Protocols were approved by the Internal Review Board of Beijing Tiantan Hospital affiliated with Capital Medical University, and the study was conducted in accordance with the principles laid down in the Declaration of Helsinki (no. KY2016-035-01).

GH3 cells were purchased from ATCC and cultured in F-12K medium (ATCC, Manassas, VA, USA) with 2.5% fetal bovine serum and 10% horse serum in a humidified incubator at 37 °C and 5% CO<sub>2</sub>.

#### 4.2. Protein Preparation and Proteomics Analysis

Protein preparation and proteomics analysis were completed in accordance with the methods used in our previous study [28]. A mass of 100 µg of each pooled sample was then denatured, reduced, and alkylated as described in the iTRAQ protocol (Thermo Fisher, Waltham, MA, USA) and digested overnight with 0.1 µg/µL trypsin solution at 37 °C. Peptides were analyzed by nanoLC-MS/MS on a Q Exactive mass spectrometer (Thermo Fisher, USA). Chromatography was performed with solvent A (Milli-Q (Millipore, Billerica, MA, USA) water with 2% acetonitrile and 0.1% formic acid) and solvent B (90% acetonitrile with 0.1% formic acid). The Q Exactive instrument was operated in information-dependent data acquisition mode to switch automatically between MS and MS/MS acquisition. MS spectra were acquired across the mass range of 350–2000 *m/z*. All MS/MS data were analyzed using Mascot (Matrix Science, London, UK; version 2.3.0). Carbamidomethylation of cysteine residues was specified as a fixed modification. Oxidation of methionine residues was specified in Mascot as a variable modification. Only proteins with a *p* < 0.05 were accepted.

#### 4.3. RNA Microarray and PCR Verification

Microarray hybridization and qRT-PCR were conducted in accordance with the methods used in our previous study [28]. Total RNA of 30 samples was extracted and purified using mirVana™ miRNA Isolation Kit (Ambion, Austin, TX, USA) following the manufacturer's instructions. Labeled cRNA was purified using an RNeasy mini kit (QIAGEN, Hilden, Germany). Each slide was hybridized with 1.65 µg Cy3-labeled cRNA using a Gene Expression Hybridization Kit (Agilent Technologies, Santa Clara, CA, USA) in a Hybridization Oven (Agilent Technologies), according to the manufacturer's instructions. After 17 h hybridization, slides were washed in staining dishes (Thermo Shandon, USA) with a Gene Expression Wash Buffer Kit (Agilent Technologies), following the manufacturer's instructions. Slides were scanned with an Agilent Microarray Scanner using default settings: Dye channel: green, scan resolution = 3 µm, PMT 100%, 20 bit. Data were extracted with Feature Extraction software 10.7 (Agilent Technologies). Raw data were normalized using the Quantile algorithm and limma package in R. The selected mRNAs were grouped into functional categories based on the Gene Ontology database (GO: <http://www.geneontology.org/>, accessed on 1 August 2022), and functional pathways (KEGG and BIOCARTA) were also analyzed using an online SAS analysis system.

qRT-PCR was performed on the Applied Bio-systems 7500 Fast System (Life Technologies, Carlsbad, CA, USA). The fold-change in differential expression for each gene was calculated using the comparative CT method ( $2^{-\Delta\Delta CT}$  method), R package: "pcr", <https://github.com/MahShaaban/pcr>, accessed on 5 May 2020 reference gene: "GAPDH," reference group: "Somatotroph Adenoma" [29].

#### 4.4. Tissue Microarray Construction and Immunohistochemistry Staining

A total of 145 formalin-fixed, paraffin-embedded tissue blocks were sliced and stained with hematoxylin–eosin, and slides were prepared. Three core biopsies, 2.0 mm in diameter, were selected from the paraffin-embedded tissue. The cores were transferred to tissue microarrays using the Minicore from Mitogen (UK). The tissue microarrays were cut into 4 µm sections. Primary antibodies anti-eIF2β (1:300, Abcam, Cambridge, UK), anti-STAT3 (1:1000, Abcam), anti-CD4 (1:300, Abcam), anti-CD8 (1:400, Abcam), anti-CD20 (1:100, LEICA, Wetzlar, Germany), anti-CD86 (1:800, Abcam), and anti-CD163 (1:600, Abcam) were used. The H-score was obtained by multiplying the staining intensity with a constant to adjust the mean to the strongest staining section (H-score = 3 × (percentage of strong staining); 1.0 (% weak), 2.0 (% moderate), 3.0 (% strong)) to give a score ranging from 0 to 300.

#### 4.5. SDS-PAGE and Western Blot Analyses

The 10 mg samples were lysed in lysate buffer containing 1% Nonidet *p*-40 (Calbiochem, Germany) with protease- and phosphatase-inhibitor cocktails (Roche) overnight at 4 °C. Total extracts were centrifuged for 30 min at 12,000× *g* and 4 °C, and protein

concentration was determined using the BCA method (Pierce Biotechnology). An aliquot of 40 µg protein per lane was loaded onto 10% Bis-Tris SDS-PAGE gels, separated electrophoretically, and blotted onto polyvinylidene fluoride (PVDF) membranes. Different blots were incubated with antibodies against anti-eIF2β (1:1000, Abcam), STAT3 (1:2000, Abcam), STAT5b (1:2000, Abcam), and GAPDH (1:8000, Sigma, St. Louis, MI, USA), followed by secondary antibodies tagged with horseradish peroxidase (Santa Cruz Biotechnology, Dallas, TX, USA). Blots were visualized by enhanced chemiluminescence, and densitometry was performed with Amersham Imager 600. Analysis of GAPDH levels was used as a loading control.

#### 4.6. Construction of Expression Plasmids and Virus Packaging

This analysis identified two stretches of 21 nucleotides in the eIF2β region as potential shRNA targeting sequences: shRNA-2: 5'-GGAGGACGACCTTGACATT-3', shRNA-3: 5'-CCCAAACATCTCCTTGACAT-3'. Scrambled targeting sequence with no known mammalian homology, 5'-GGATTGATTCAACACGGAAGA-3', was used as the negative control. DNA oligonucleotides were synthesized, annealed, and cloned into Plvx-shRNA2-ZsGreen1-T2A-Puro (Oligobio, Beijing, China). The inserts of the clones were verified by PCR and sequencing. Positive viruses for eIF2β shRNA and control shRNA expression were named sh2 and sh3, respectively. Plvx-shRNA2-T2A-puro-eIF2β vector supernatants were generated by co-transfecting 15 µg Plvx-shRNA2-T2A-puro shRNA vector, 11.25 µg of psPAX2 transfer vector, and 3.75 µg of Pmd2.G into HEK293T cells in a 12-well plate using linear PEI reagent. Supernatants were collected at 48 h after transfection and filtered through a 0.45 µm polyvinylidene fluoride (PVDF) syringe filter (Corning Life Sciences, Tewksbury, MA, USA). To determine the titer, we infected  $3 \times 10^4$  cells in a 48-well plate with serial dilutions of the Plvx-shRNA2-T2A-puro-eIF2β vector supernatants in the presence of polybrene (10 µL) (Sigma-Aldrich, St. Louis, MO, USA) and analyzed them 3 days post-transduction by flow cytometry analysis using the BD FACS Fortessa (BD Biosciences, San Jose, CA, USA). Transductions of HEK293T cell lines were performed on  $2 \times 10^4$  cells/well in a 24-well plate followed by flow cytometric analysis of Venus expression 3 days post-transduction.

#### 4.7. Cell Proliferation and Migration Assays

GH3 cells were adjusted to a density of  $1 \times 10^5$  cells/mL. An aliquot of 100 µL of cell suspension was plated into each well of 96-well plates and cultured overnight. At 24, 48, and 72 h post-transfection, 20 µL 3-(4,5-diethylthiazol-2-yl)-5-(3-carboxymethoxyphenyl)-2-(4-sulfophenyl)-2H-tetrazolium inner salt (MTS) solution was added to each well, followed by further incubation for 4 h. Absorbance of each well at 490 nm was measured using an ELISA plate reader (Thermo, USA). Cell migration was measured using fibronectin and Matrigel-coated polycarbonate filters, respectively, and modified transwell chambers (Corning, MA, USA). GH3 cells ( $5 \times 10^4$  cells) were added into the upper chambers. After 24 h of incubation, migrating cells that adhered to the lower membrane were fixed in 4% paraformaldehyde and stained using hematoxylin (Zhongshan Company, Beijing, China). No invading cells were removed with cotton swabs. Images were photographed in three randomly selected fields of view at 200× magnification. Experiments were performed in triplicate.

#### 4.8. ELISA

The levels of GH and IGF-1 were detected using an ELISA kit (APPLYGEN) according to the protocol. An aliquot of 10 µL of cell culture supernatant per well was used. The absorbance of each well was measured at 450 nm using an ELISA plate reader (Thermo Fisher). The amount of GH and IGF-1 was calculated from a standard curve prepared using the recombinant protein. Positive controls were supplied in the kit.

#### 4.9. Statistical Analysis

Chi-square test and Fisher's exact test were used to determine the significance of categorical variables. One-way ANOVA was applied to the immunohistochemical results in patients or in vitro experiments. All *p* values are two-sided, and 0.05 was applied as the significance level.

**Supplementary Materials:** The following supporting information can be downloaded at: <https://www.mdpi.com/article/10.3390/ijms232113067/s1>.

**Author Contributions:** Conceptualization, H.G.; methodology, X.Y. and Q.L.; validation, H.Z.; formal analysis, Y.C.; investigation, Z.L.; resources, Y.Z.; data curation, Y.C.; writing—original draft preparation, Z.L.; writing—review and editing, J.F.; project administration, H.G. All authors have read and agreed to the published version of the manuscript.

**Funding:** This work was financially supported by the Natural Foundation project of The Applied Basic Research Program of Shanxi Province (201901D111430), the Beijing Municipal Health Commission (11000022T00000423806), and the National Natural Science Foundation of China (81601205). The present study was supported by the National Natural Science Foundation of China (81771489).

**Institutional Review Board Statement:** This study was conducted according to the guidelines of the Declaration of Helsinki and approved by the Institutional Review Board Beijing of Tiantan Hospital, affiliated with Capital Medical University (No. KY2016-035-01).

**Informed Consent Statement:** Informed consent was obtained from all subjects involved in the study.

**Data Availability Statement:** All the data generated or analyzed in this study are included in this published article and its additional files.

**Acknowledgments:** The authors would like to thank the pathologists, Guilin Li and Yanjiao He, as well as the laboratory technicians, data collectors, and medical editors.

**Conflicts of Interest:** The authors declare no conflict of interest.

## References

1. Molitch, M.E. Diagnosis and Treatment of Pituitary Adenomas: A Review. *JAMA* **2017**, *317*, 516–524. [[CrossRef](#)] [[PubMed](#)]
2. Giustina, A.; Barkhoudarian, G.; Beckers, A.; Ben-Shlomo, A.; Biermasz, N.; Biller, B.; Boguszewski, C.; Bolanowski, M.; Bollerslev, J.; Bonert, V.; et al. Multidisciplinary Management of Acromegaly: A Consensus. *Rev. Endocr. Metab. Disord.* **2020**, *21*, 667–678. [[CrossRef](#)] [[PubMed](#)]
3. Colao, A.; Grasso, L.F.S.; Giustina, A.; Melmed, S.; Chanson, P.; Pereira, A.M.; Pivonello, R. Acromegaly. *Nat. Rev. Dis. Primers* **2019**, *5*, 20. [[CrossRef](#)] [[PubMed](#)]
4. Wolters, T.L.C.; Netea, M.G.; Riksen, N.P.; Hermus, A.R.M.M.; Netea-Maier, R.T. Acromegaly, Inflammation and Cardiovascular Disease: A Review. *Rev. Endocr. Metab. Disord.* **2020**, *21*, 547–568. [[CrossRef](#)] [[PubMed](#)]
5. Sahin, S.; Icli, T.B.; Durcan, E.; Sulu, C.; Ozkaya, H.M.; Hatemi, A.I.; Kadioglu, P. The Effect of Somatostatin Analogs and Acromegaly on the Upper Gastrointestinal System. *Pituitary* **2021**, *24*, 184–191. [[CrossRef](#)] [[PubMed](#)]
6. Kontogeorgos, G.; Thodou, E.; Osamura, R.Y.; Lloyd, R.V. High-Risk Pituitary Adenomas and Strategies for Predicting Response to Treatment. *Hormones* **2022**, *21*, 1–14. [[CrossRef](#)] [[PubMed](#)]
7. Costa-Mattioli, M.; Walter, P. The Integrated Stress Response: From Mechanism to Disease. *Science* **2020**, *368*, eaat5314. [[CrossRef](#)]
8. Tian, X.; Zhang, S.; Zhou, L.; Seyhan, A.A.; Hernandez Borrero, L.; Zhang, Y.; El-Deiry, W.S. Targeting the Integrated Stress Response in Cancer Therapy. *Front. Pharmacol.* **2021**, *12*, 747837. [[CrossRef](#)]
9. Hinnebusch, A.G.; Ivanov, I.P.; Sonenberg, N. Translational Control by 5'-Untranslated Regions of Eukaryotic MRNAs. *Science* **2016**, *352*, 1413–1416. [[CrossRef](#)]
10. Adomavicius, T.; Guaita, M.; Zhou, Y.; Jennings, M.D.; Latif, Z.; Roseman, A.M.; Pavitt, G.D. The Structural Basis of Translational Control by EIF2 Phosphorylation. *Nat. Commun.* **2019**, *10*, 2136. [[CrossRef](#)]
11. Duggimpudi, S.; Kloetgen, A.; Maney, S.K.; Münch, P.C.; Hezaveh, K.; Shaykhalishahi, H.; Hoyer, W.; McHardy, A.C.; Lang, P.A.; Borkhardt, A.; et al. Transcriptome-Wide Analysis Uncovers the Targets of the RNA-Binding Protein MSI2 and Effects of MSI2's RNA-Binding Activity on IL-6 Signaling. *J. Biol. Chem.* **2018**, *293*, 15359–15369. [[CrossRef](#)] [[PubMed](#)]
12. Schmidt, S.; Gay, D.; Uthe, F.W.; Denk, S.; Paauwe, M.; Matthes, N.; Diefenbacher, M.E.; Bryson, S.; Warrander, F.C.; Erhard, F.; et al. A MYC-GCN2-EIF2 $\alpha$  Negative Feedback Loop Limits Protein Synthesis to Prevent MYC-Dependent Apoptosis in Colorectal Cancer. *Nat. Cell. Biol.* **2019**, *21*, 1413–1424. [[CrossRef](#)] [[PubMed](#)]

13. Nguyen, H.G.; Conn, C.S.; Kye, Y.; Xue, L.; Forester, C.M.; Cowan, J.E.; Hsieh, A.C.; Cunningham, J.T.; Truillet, C.; Tameire, F.; et al. Development of a Stress Response Therapy Targeting Aggressive Prostate Cancer. *Sci. Transl. Med.* **2018**, *10*, eaar2036. [[CrossRef](#)] [[PubMed](#)]
14. Komar, A.A.; Merrick, W.C. A Retrospective on EIF2A-and Not the Alpha Subunit of EIF2. *Int. J. Mol. Sci.* **2020**, *21*, E2054. [[CrossRef](#)] [[PubMed](#)]
15. Jewer, M.; Lee, L.; Leibovitch, M.; Zhang, G.; Liu, J.; Findlay, S.D.; Vincent, K.M.; Tandoc, K.; Dieters-Castator, D.; Quail, D.F.; et al. Translational Control of Breast Cancer Plasticity. *Nat. Commun.* **2020**, *11*, 2498. [[CrossRef](#)] [[PubMed](#)]
16. Vanselow, S.; Neumann-Arnold, L.; Wojciech-Moock, F.; Seufert, W. Stepwise Assembly of the Eukaryotic Translation Initiation Factor 2 Complex. *J. Biol. Chem.* **2022**, *298*, 101583. [[CrossRef](#)] [[PubMed](#)]
17. Mellado, W.; Willis, D.E. Stressing out Translation. *Science* **2021**, *373*, 1089–1090. [[CrossRef](#)]
18. Ghaddar, N.; Wang, S.; Woodvine, B.; Krishnamoorthy, J.; van Hoef, V.; Darini, C.; Kazimierczak, U.; Ah-Son, N.; Popper, H.; Johnson, M.; et al. The Integrated Stress Response Is Tumorigenic and Constitutes a Therapeutic Liability in KRAS-Driven Lung Cancer. *Nat. Commun.* **2021**, *12*, 4651. [[CrossRef](#)]
19. Licari, E.; Sánchez-Del-Campo, L.; Falletta, P. The Two Faces of the Integrated Stress Response in Cancer Progression and Therapeutic Strategies. *Int. J. Biochem. Cell Biol.* **2021**, *139*, 106059. [[CrossRef](#)]
20. Schoof, M.; Boone, M.; Wang, L.; Lawrence, R.; Frost, A.; Walter, P. EIF2B Conformation and Assembly State Regulate the Integrated Stress Response. *Elife* **2021**, *10*, e65703. [[CrossRef](#)]
21. Donnelly, N.; Gorman, A.M.; Gupta, S.; Samali, A. The EIF2 $\alpha$  Kinases: Their Structures and Functions. *Cell Mol. Life Sci.* **2013**, *70*, 3493–3511. [[CrossRef](#)] [[PubMed](#)]
22. Gatza, M.L.; Silva, G.O.; Parker, J.S.; Fan, C.; Perou, C.M. An Integrated Genomics Approach Identifies Drivers of Proliferation in Luminal-Subtype Human Breast Cancer. *Nat. Genet.* **2014**, *46*, 1051–1059. [[CrossRef](#)] [[PubMed](#)]
23. Tanaka, I.; Sato, M.; Kato, T.; Goto, D.; Kakumu, T.; Miyazawa, A.; Yogo, N.; Hase, T.; Morise, M.; Sekido, Y.; et al. EIF2 $\beta$ , a Subunit of Translation-Initiation Factor EIF2, Is a Potential Therapeutic Target for Non-Small Cell Lung Cancer. *Cancer Sci.* **2018**, *109*, 1843–1852. [[CrossRef](#)] [[PubMed](#)]
24. Salton, G.D.; Laurino, C.C.F.C.; Mega, N.O.; Delgado-Cañedo, A.; Setterblad, N.; Carmagnat, M.; Xavier, R.M.; Cirne-Lima, E.; Lenz, G.; Henriques, J.A.P.; et al. Deletion of EIF2 $\beta$  Lysine Stretches Creates a Dominant Negative That Affects the Translation and Proliferation in Human Cell Line: A Tool for Arresting the Cell Growth. *Cancer Biol Ther.* **2017**, *18*, 560–570. [[CrossRef](#)] [[PubMed](#)]
25. Gordiyenko, Y.; Llácer, J.L.; Ramakrishnan, V. Structural Basis for the Inhibition of Translation through EIF2 $\alpha$  Phosphorylation. *Nat. Commun.* **2019**, *10*, 2640. [[CrossRef](#)] [[PubMed](#)]
26. Zhou, C.; Jiao, Y.; Wang, R.; Ren, S.-G.; Wawrowsky, K.; Melmed, S. STAT3 Upregulation in Pituitary Somatotroph Adenomas Induces Growth Hormone Hypersecretion. *J. Clin. Investig.* **2015**, *125*, 1692–1702. [[CrossRef](#)] [[PubMed](#)]
27. Lu, J.-Q.; Adam, B.; Jack, A.S.; Lam, A.; Broad, R.W.; Chik, C.L. Immune Cell Infiltrates in Pituitary Adenomas: More Macrophages in Larger Adenomas and More T Cells in Growth Hormone Adenomas. *Endocr. Pathol.* **2015**, *26*, 263–272. [[CrossRef](#)] [[PubMed](#)]
28. Feng, J.; Wang, J.; Liu, Q.; Li, J.; Zhang, Q.; Zhuang, Z.; Yao, X.; Liu, C.; Li, Y.; Cao, L.; et al. DAPT, a  $\gamma$ -Secretase Inhibitor, Suppresses Tumorigenesis, and Progression of Growth Hormone-Producing Adenomas by Targeting Notch Signaling. *Front. Oncol.* **2019**, *9*, 809. [[CrossRef](#)]
29. Chen, Y.; Li, B.; Feng, J.; Fang, Q.; Cheng, J.; Xie, W.; Li, C.; Cheng, S.; Zhang, Y.; Gao, H. JAG1, Regulated by MicroRNA-424-3p, Involved in Tumorigenesis and Epithelial-Mesenchymal Transition of High Proliferative Potential-Pituitary Adenomas. *Front. Oncol.* **2020**, *10*, 567021. [[CrossRef](#)]